# Electron Spin Resonance and Electron Spin Echo Modulation Studies on Reducibility, Location, and Adsorbate Interactions of Ni(I) in Ni(II)-Exchanged SAPO-34

**Marie-Ange Djieugoue, A. M. Prakash, and Larry Kevan***

*Department of Chemistry, University of Houston, Houston, Texas 77204-5641*

*Received: February 5, 1998; In Final Form: April 6, 1998*

Electron spin resonance (ESR) and electron spin echo modulation (ESEM) spectroscopies were used to study the reducibility, location, and adsorbate interactions of Ni(I) in NiH−SAPO-34, in which Ni(II) was introduced into extraframework sites of SAPO-34 by partial ion exchange of H(I) by Ni(II). After dehydration at temperatures above 573 K as well as after $\gamma$-irradiation at 77 K, one nickel species assigned as isolated Ni(I) by ESR is observed. Along with the isolated Ni(I) species, a second species assigned to Ni(I)−$(H_2)_n$ is also observed after hydrogen reduction at 573 K. Adsorption of water into reduced NiH−SAPO-34 forms an axially symmetric Ni(I)−$(O_2)_n$ complex indicating water decomposition by Ni(I). Adsorption of methanol into reduced NiH−SAPO-34 forms two Ni(I)-methanol complexes suggested to be located at two different sites in the chabazite structure. Similarly, two Ni(I)−$(C_2D_4)_n$ complexes, the predominant one exhibiting axial symmetry and the other one having rhombic symmetry, are formed after ethylene adsorption onto reduced NiH−SAPO-34. Analysis of the $^{13}$C hyperfine structure obtained after $^{13}$CO adsorption showed a Ni(I)−$(CO)_3$ species. The location of Ni(I) in NiH−SAPO-34 was determined qualitatively by $^{27}$Al ESEM which suggested that even though Ni is situated within 5 Å of the framework aluminum, the two species are not in close proximity. A more quantitative analysis using $^{31}$P ESEM showed that Ni(I) is at site II′ in the chabazite cage near a six-ring window after both thermal and hydrogen reduction.

## Introduction

Silicoaluminophosphate (SAPO) materials discovered in 1984 at Union Carbide belong to a class of crystalline microporous molecular sieves.[1] Their tetrahedral oxide frameworks containing silicon, aluminum, and phosphorus atoms can be viewed in terms of silicon substitution into aluminophosphate frameworks. They exhibit properties both of zeolites and of aluminophosphates yet are unique in many ways. Some of these properties, such as adsorbents for separation and purification of molecular species, catalysts, or catalyst supports, and ion-exchange agents are a consequence of the fact that the framework phosphorus substitution by silicon creates a net negative framework charge which is balanced by $H^+$ ions after calcination. The fact that the $H^+$ ions can be partially exchanged by a transition-metal ion makes SAPO materials interesting candidates for several catalytic reactions. Cu-exchanged SAPO molecular sieves have been reported to be thermostable catalysts for selective reduction of $NO_x$ with hydrocarbons.[2] Of the various catalysts tested, including SAPO-5, SAPO-11, SAPO-34, beta, USY, and ZSM-5, Cu−SAPO-34 was found to exhibit the highest activity for NO reduction at temperatures above 973 K. Nickel-modified SAPO-34 has been shown to be a highly efficient catalyst for the selective conversion of methanol to ethene.[3]

Silicoaluminophosphate type 34 (SAPO-34) is a cage type molecular sieve with framework structure similar to the naturally occurring zeolite chabazite.[1,4,5] This is a small pore molecular sieve, the structure of which is composed of hexagonal prisms joined together by four-membered rings to form a large ellipsoidal cavity. Each cavity is connected with six identical cavities through eight-membered tetrahedral rings with an effective diameter of about 3.8 Å.[4,6] SAPO-34 in its protonic form has been reported to be a very efficient catalyst for the reaction of methanol to olefins (MTO).[7]

Nickel-modified molecular sieves have proven to be active catalysts in reactions such as acetylene cyclomerization and ethylene and propylene oligomerization.[8,9] Monovalent nickel is found to be the active species in these reactions. Monovalent nickel in Ni(II)-exchanged SAPO materials can be achieved using several reduction methods such as thermal treatment, photoirradiation by ultraviolet light, hydrogen or carbon monoxide treatment, and $\gamma$-irradiation.[10,11] Since the catalytic properties of nickel-exchanged SAPO and zeolite materials are strongly dependent on the nature and location of the Ni ions as well as their accessibility and coordination with ligands, it is important to elucidate the location of the ions within the molecular sieve structure and the number and orientation of adsorbate molecules coordinating to them. In the past, electron spin resonance (ESR) and electron spin echo (ESEM) spectroscopies have been used effectively to probe the nature of incorporated Ni species in both framework and extraframework positions in SAPO materials such as SAPO-5, -11, and -41.[12−14] Even though nickel-modified SAPO-34 has shown to be a highly efficient catalyst, little has been reported on the nature of Ni in this material. In this work, after hydrothermal synthesis of SAPO-34 and solid-state ion exchange with Ni(II), the reducibility of Ni(II) and the interaction of Ni(I) with various adsorbates are investigated using ESR. As a supplement to this, ESEM of $^{31}$P and $^{27}$Al are used to ascertain the location of the incorporated paramagnetic transition-metal ion.

## Experimental Section

**Synthesis.** SAPO-34 was prepared hydrothermally with morpholine being used as the templating agent.[15] The following chemicals were used without further purification: phosphoric acid (85%, Mallinckrodt), pseudoboehmite (Catapal B, Vista), fumed silica (Sigma), morpholine (99%, Aldrich), nickel chloride hexahydrate (Aldrich). The synthesis was carried out in a 100 $cm^3$ stainless steel reactor lined with Teflon at

S1089-5647(98)01037-2 CCC: $15.00 
Published on Web 05/07/1998

autogenous pressure without agitation. The molar composition of the reaction mixture for the preparation of SAPO-34 was 1.0 $Al_2O_3$:1.0 $P_2O_5$:0.6 $SiO_2$:2.0 R:60 $H_2O$ where R stands for the template. In a typical synthesis, 10 mL of water was added to 5.83 g of pseudoboehmite, and then 9.27 g of phosphoric acid and another 10 mL of water were added dropwise to the first mixture over a period of 2 h. After stirring the resultant mixture for another 2 h, 1.44 g of fumed silica and 10 mL of water were added slowly and stirred for 30 min. Finally, 7.04 g of morpholine and another 10 mL of water were added dropwise. The gel was then stirred for 24 h at room temperature for aging. The final gel was put into an autoclave and heated to 473 K for 48 h. After crystallization, the product was separated from the mother liquor, washed repeatedly with water, and dried at 373 K overnight. The as-synthesized product was then slowly heated to 823 K in $O_2$ and kept at this temperature for 12 h in order to completely remove the organic template.

NiH−SAPO-34, in which Ni(II) ions are in extraframework positions, was prepared by solid-state ion exchange using $NiCl_2 \cdot 6H_2O$ and H−SAPO-34. A mixture of 0.03 g of nickel chloride and 2 g of H−SAPO-34 was ground in a mortar with a pestle for 30 min. This solid mixture was then heated in an oven at 873 K in $O_2$ for 12 h and slowly cooled to room temperature. Before and after solid-state ion exchange, the sample remained white. The idealized chemical composition of this sample was $Ni_{0.002}Si_{0.037}Al_{0.50}P_{0.46}$ based on electron probe microanalysis.

**Sample Treatment and Measurement.** For ESR and ESEM measurements, calcined and hydrated samples were loaded into 3 mm o.d. by 2 mm i.d. Suprasil quartz tubes and gradually heated under vacuum ($<10^{-4}$ Torr) to 373 K. The samples were then kept at this temperature for 12 h. The most common and most stable oxidation state of Ni is Ni(II), $3d^8$, which is not paramagnetic. Our goal is to generate paramagnetic Ni(I) by reducing the Ni(II). To study the behavior of nickel as a function of dehydration, the samples were slowly heated under vacuum from 373 to 773 K at intervals of 100 K. This procedure accomplishes thermal reduction. ESR spectra were recorded at 77 K to detect the formation of any Ni(I) species. In another reduction method known as hydrogen reduction, the samples were first dehydrated to 773 K as described above, contacted with 500 Torr of dry $O_2$ at room temperature, and then heated to 823 K for overnight. The oxygen treatment was used to reoxidize any reduced Ni(I) ions to Ni(II). After that, the samples were contacted with dry $H_2$ at room temperature and subsequently heated to 573 K for not more than 1 h to avoid further reduction of Ni(I) to Ni(0). Special care was taken to ensure that both the vacuum line and the hydrogen gas were water-free because of the high reactivity of Ni(I) toward even traces of water. Samples were frozen in liquid nitrogen for ESR measurements. A third reduction method called $\gamma$-ray reduction consisted in sealing the dehydrated samples, placing them in liquid nitrogen, and exposing them to $\gamma$-radiation from a $^{60}Co$ source at a dose rate of 0.2 Mrad/h. The total exposure time was 6 h, and the total dose was 1.2 Mrad. It is important to note that although this reduction method considerably enhances the isolated Ni(I) signal, it can also generate other paramagnetic centers. To prepare Ni(I) complexes with various adsorbates, the hydrogen-reduced samples were evacuated and then exposed to the room-temperature vapor pressure of $D_2O$ (Aldrich), $CD_3$-OH (Stohler Isotope Chemicals), 100 Torr of $C_2D_4$ (Cambridge Isotope Laboratories), 100 Torr of $^{12}CO$ (Cambridge), and 100 Torr of $^{13}CO$ (Stable Isotopes). These samples were frozen in liquid nitrogen and sealed. The samples remained white after these treatments.

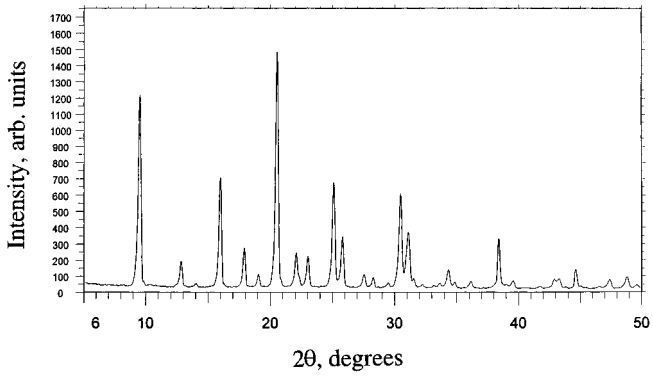


**Figure 1.** X-ray powder diffraction pattern for as-synthesized SAPO-34.

ESR spectra were recorded with a Bruker ESP-300 X-band spectrometer at 77 K. The magnetic field was calibrated with a Varian E-500 gaussmeter. The microwave frequency was measured by a Hewlett-Packard HP 5342A frequency counter. ESEM spectra were measured at 4.8 K with a Bruker ESP 380 pulsed ESR spectrometer. Three-pulse echoes were measured by using a $\tau/2-\tau-\tau/2-T-\tau/2$ pulse sequence as a function of time $T$ to obtain the time domain spectrum. $^{31}P$ modulation was obtained with a $\tau$ value of 0.28 $\mu$s to minimize $^{27}Al$ modulation. Modulation from $^{27}Al$ was monitored with $\tau$ = 0.40 $\mu$s, which is the optimal value for recording the deepest $^{27}Al$ modulation. The phosphorus modulation was analyzed by a spherical approximation for powder samples in terms of N nuclei at distance $R$ with an isotropic hyperfine coupling $A_{iso}$. The best fit simulation of an ESEM signal is found by varying the parameters until the sum of the squared residuals is minimized.

## Results

**X-ray Powder Diffraction.** Figure 1 shows the powder XRD pattern of SAPO-34 in its as-synthesized form. This pattern matches in both intensity and line position the pattern reported[16] and confirms that the material obtained is indeed of pure phase. No loss in crystallinity is observed when the as-synthesized sample is calcined at 823 K to remove the organic species.

**Electron Spin Resonance.** Calcined NiH−SAPO-34 did not show any ESR signal at 77 K. We therefore assume that the Ni species is in the form Ni(II). Figure 2 shows the behavior of NiH−SAPO-34 as a function of dehydration. The sample was held at each temperature for 12 h. Dehydration below 573 K produced no paramagnetic species. Upon dehydration of the sample at 573 K, two paramagnetic species, denoted A and B, are observed. Species A has axial symmetry with $g_{\parallel}^{A} = 2.651$ and $g_{\perp}^{A} = 2.096$, and species B is broader with rhombic $g$ parameters $g_1^{B} = 1.998$, $g_2^{B} = 1.967$, ad $g_3^{B} = 1.936$. Dehydration at higher temperatures reduces the intensity of species A, while the intensity of species B remains more or less the same. Species A is assigned to isolated Ni(I) formed by desorbing water and hydroxyl groups.[17] The ESR parameters of species A observed in NiH−SAPO-34 are somewhat lower than those reported for Ni(I) in NiH−SAPO-5,[18] NiH−SAPO-11, and NiH−SAPO-41.[19] Species B has been observed in NiH−SAPO-5 where it could also be seen in the absence of nickel in H−SAPO-5 after dehydration at 673 K in vacuum. Species B has also been observed in several other AlPO-*n* materials after dehydration and was assigned to some type of framework defect.[20]

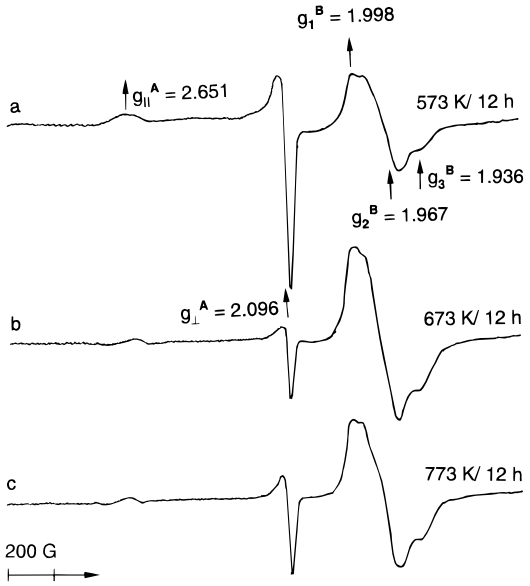


**Figure 2.** ESR spectra at 77 K of NiH−SAPO-34 (a) after dehydration at 573 K for 12 h, (b) after dehydration at 673 K for 12 h, and (c) after dehydration at 773 K for 12 h.

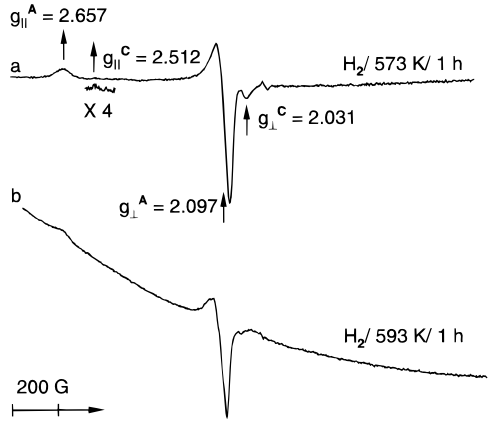


**Figure 3.** ESR spectra at 77 K of NiH−SAPO-34 (a) after $H_2$ treatment of a dehydrated sample at 573 K for 1 h and (b) after $H_2$ treatment of a dehydrated sample at 593 K for 1 h.

Figure 3a shows the ESR spectrum of NiH−SAPO-34 after hydrogen reduction at 573 K for 1 h. Two Ni(I) species, denoted A and C, are observed. Species A is the same as already observed after thermal reduction. Upon evacuation of the hydrogen at room temperature, species A remains whereas the axially symmetric species C with ESR parameters $g_{||}^C = 2.512$ and $g_\perp^C = 2.031$ disappears but is regenerated if the sample is again exposed to hydrogen. Therefore, species C is ascribed to Ni(I)−$(H_2)_n$. The same behavior has been reported in NiH−SAPO-5, NiH−SAPO-11, and NiH−SAPO-41. It is important to note that formation of Ni(I) by hydrogen reduction is highly sensitive to temperature and time. In fact, increasing the reduction temperature by only 20 K or the reduction time by 10 min leads to the formation of a broad signal due to metallic nickel (Figure 3b), suggesting that Ni(I) further reduces to Ni(0).

Ni(I) signals can also be generated in NiH−SAPO-34 by $\gamma$-irradiation at 77 K. Figure 4 shows the ESR spectrum obtained after irradiation of a dehydrated sample. The intensity of species A produced by this method is considerably higher than the corresponding signal intensity for this species after thermal or hydrogen reduction. In addition to species A, a strong signal (species D) is observed at $g = 2.009$. This signal

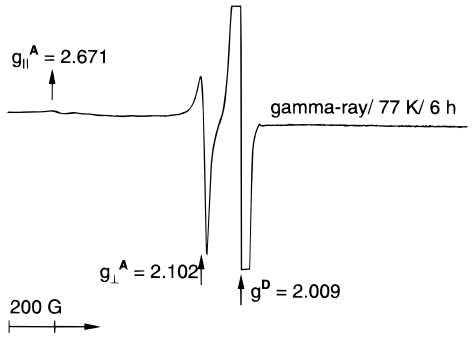


**Figure 4.** ESR spectrum at 77 K of NiH−SAPO-34 after $\gamma$-irradiation of a dehydrated sample for 6 h at 77 K.

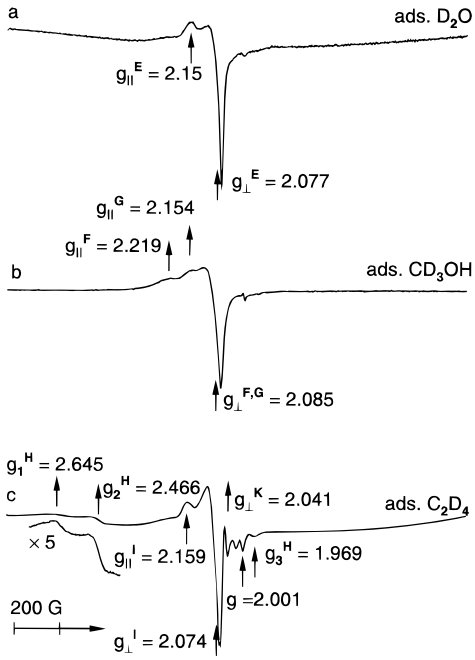


**Figure 5.** ESR spectra at 77 K of NiH−SAPO-34 (a) after $D_2O$ adsorption on a hydrogen-reduced sample at room temperature for 2 min, (b) after $CD_3OH$ adsorption on a hydrogen-reduced sample at room temperature for 2 min, and (c) after $C_2D_4$ adsorption on a hydrogen-reduced sample at room temperature for 2 min.

has been reported earlier in Y zeolite and SAPO-41 to be a V center due to trapped holes on oxygen bonded to aluminum or silicon. An unstable species characterized by a doublet split by 500 G due to trapped hydrogen atoms in the quartz sample tube wall can also be seen when the sample is measured immediately after exposure to the radiation. Even though $\gamma$-irradiation enhances species A, the presence of the very strong signal due to V centers makes this reduction method not suitable to study adsorbate interactions.

**Adsorbate Interactions.** Before an adsorbate was added, the hydrogen-reduced samples were evacuated for 5 min at room temperature so only isolated Ni(I) remains. The sample was then exposed to the adsorbate at room temperature for no more than 3 min because of the high instability of Ni(I) at this temperature, quenched in liquid nitrogen before being taken for ESR measurement.

Deuterated water adsorption on NiH−SAPO-34 produces a single species E with axial symmetry and ESR parameters $g_{||}^E = 2.150$ and $g_\perp^E = 2.077$ (Figure 5a). A species with somewhat similar $g$ values and rhombic symmetry has been reported earlier in NiH−SAPO-11, NiH−SAPO-5, NiH−SAPO-41, and NiCa−Y zeolite[21] and was assigned to Ni(I)−$(O_2)_n$ produced by decomposition of water on Ni(I) sites. However, the axial symmetry

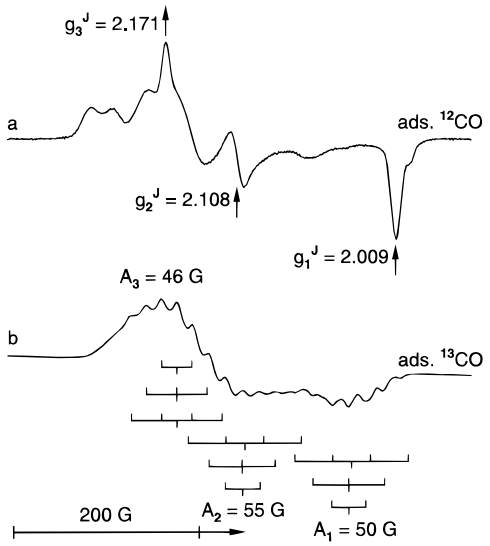


**Figure 6.** ESR spectra at 77 K of NiH−SAPO-34 (a) after $^{12}$CO adsorption on a hydrogen-reduced sample at room temperature for 2 min and (b) after $^{13}$CO adsorption on a hydrogen-reduced sample at room temperature for 2 min.

of species E in SAPO-34 is unusual. This assignment of species E to a Ni(I)−$(O_2)_n$ complex is based on two observations. First of all, adsorption of $O_2$ instead of $D_2O$ led to the same species. Second, ESEM at $g_\perp^E = 2.077$ showed no deuterium modulation to assign this species to a possible Ni(I)−$(D_2O)_n$ complex.

Adsorption of methanol on NiH−SAPO-34 produced two axially symmetric species F and G with different parallel components $g_\parallel^F = 2.219$ and $g_\parallel^G = 2.154$ but the same perpendicular component $g_\perp^{F,G} = 2.085$ (Figure 5b). The fact that the ESR parameters are different from those of the hydrogen-reduced sample shows evidence of methanol coordination. The observation of two species suggests two locations within the SAPO-34 structure for the Ni(I)−$(CD_3OH)_n$ complex. This behavior has not been reported in previous SAPO materials, indicating that this pattern is closely associated with the structure of SAPO-34.

Figure 5c is obtained after adsorption of 100 Torr of ethylene at room temperature on NiH−SAPO-34 containing Ni(I). An axially symmetric species I with $g_\parallel^I = 2.159$ and $g_\perp^I = 2.074$ appears as the predominant feature of this figure. Less intense species include a rhombic species designated as species H with ESR parameters $g_1^H = 2.645$, $g_2^H = 2.466$, and $g_3^H = 1.969$ and a species K with $g_\perp^K = 2.041$. Species I and H are assigned as two Ni(I)−$(C_2H_4)_n$ complexes located within the chabazite cage. Species K probably results from the interaction of species A with the butene product of ethylene dimerization. An ethylene complex similar to species H has been reported earlier in NiCa−X,[22] NiLa−Y,[23] and NiH−SAPO-11. Another species at $g = 2.001$ is also been and can be assigned to an $O_2^-$ radical.

Figure 6a shows the adsorption of 100 Torr of $^{12}$CO on NiH−SAPO-34. A species J characterized by a rhombic symmetry and **g**-tensor components $g_1^J = 2.009$, $g_2^J = 2.108$, and $g_3^J = 2.171$ can be distinguished. $^{12}$C has a nuclear spin of 0 and therefore cannot give rise to hyperfine structure. To identify species J, the same experiment was performed using 90% $^{13}$C-enriched CO. From Figure 6b, it appears that Ni(I) interacts with the nuclear spin of $^{13}$C ($I = {}^1/_2$), leading to a hyperfine structure for the Ni(I) carbonyl species. It can be observed that each of the $g$ components is split into a number of lines. Analysis of the spectrum gives the following hyperfine tensor, $A_1 = 50$ G, $A_2 = 55$ G, and $A_3 = 46$ G. Two factors lead to the assignment of species J to a tricarbonyl Ni(I)−$(CO)_3$ complex. First of all, it is reasonable to assume that the maximum number of CO molecules thought to coordinate to Ni(I) is three since Ni(I) is already bonded to three framework oxygens. Second, the splitting of the $g_1$ component was used since overlap between the $g_2$ and $g_3$ lines makes them more difficult to analyze. Doublets, triplets, and quadruplets with respective relative intensities 1:1, 1:2:1, and 1:3:3:1 are highlighted in Figure 6b representing Ni(I)−$(CO)_3$ complexes with one, two, and three $^{13}$CO. Very similar behavior has been reported for CO adsorbed on NiCa−X zeolite.[24] Table 1 summarizes the ESR parameters assigned to the various Ni(I) species observed in NiH−SAPO-34 and their assignments.

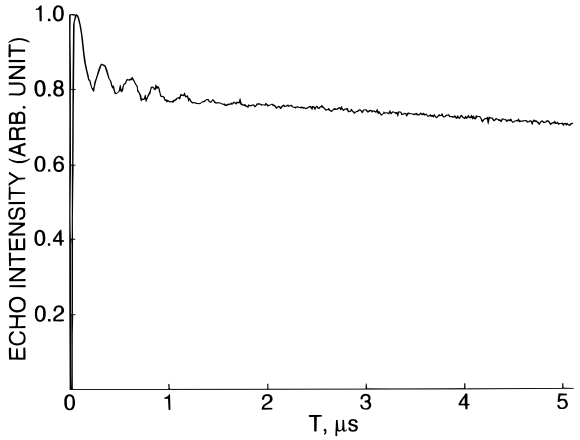


**Figure 7.** Experimental three-pulse $^{27}$Al ESEM spectrum of dehydrated NiH−SAPO-34 at the magnetic field corresponding to $g_\perp$ of Ni(I) species A.

**TABLE 1: ESR *g* Values of Ni(I) Species in NiH−SAPO-34 Produced after Various Reduction Methods and after Adsorbate Interactions**

| reduction method | adsorbate | assignment | $g_\parallel$ or $g_1$ | $g_\perp$ or $g_2$ | $g_3$ |
|---|---|---|---|---|---|
| thermal | none | Ni(I) | 2.651 | 2.096 | |
| $H_2$ | none | Ni(I) | 2.657 | 2.097 | |
| | | Ni(I)−$(H_2)_n$ | 2.512 | 2.031 | |
| $\gamma$-ray | none | Ni(I) | 2.671 | 2.102 | |
| $H_2$ | $D_2O$ | Ni(I)−$(O_2)_n$ | 2.150 | 2.077 | |
| $H_2$ | $CD_3OH$ | Ni(I)−$(CD_3OH)_n$ | 2.219 | 2.085 | |
| | | Ni(I)−$(CD_3OH)_n$ | 2.154 | 2.085 | |
| | $C_2D_4$ | Ni(I)−$(C_2D_4)_n$ | 2.159 | 2.074 | |
| | | Ni(I)−$(C_2D_4)_n$ | 2.645 | 2.466 | 1.969 |
| | | Ni(I)−$(C_4D_8)_n$ | | 2.041 | |
| $H_2$ | CO | Ni(I)−$(CO)_3$ | 2.009 | 2.108 | 2.171 |

**Electron Spin Echo Modulation.** Figure 7 illustrates the $^{27}$Al ESEM spectrum of NiH−SAPO-34 after hydrogen reduction and subsequent evacuation. The magnetic field was set at the value corresponding to the perpendicular component of Ni(I) species A. Figure 8 shows the $^{31}$P ESEM spectrum of NiH−SAPO-34 after dehydration and after hydrogen reduction. The spectra were recorded at a magnetic field corresponding to the perpendicular component of species A. The simulation parameters are given in Table 2. Upon analysis of the $^{31}$P modulation of the Ni(I) species, it is possible to identify the probable cation location in both dehydrated and hydrogen-reduced NiH−SAPO-34.

## Discussion

Several cation sites can be identified in SAPO-34. Based on the structural model of SAPO-34 and by analogy with the cation positions in the analogous zeolite chabazite,[25] major

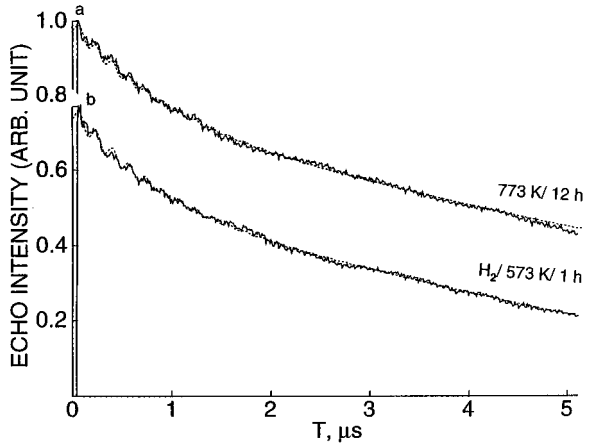


**Figure 8.** Experimental (—) and simulated (···) three-pulse $^{31}$P ESEM of NiH−SAPO-34 at the magnetic field corresponding to $g_\perp$ of Ni(I) species A (a) after dehydration at 773 K for 12 h and (b) after $H_2$ reduction at 573 K for 1 h.

**TABLE 2: $^{31}$P ESEM Parameters for Ni(I) Species in Dehydrated and Hydrogen-Reduced NiH−SAPO-34**

| reduction method | shell | N[a] | R[b], nm | $A_{iso}$,[c] MHz |
|---|---|---|---|---|
| thermal | 1 | 2.2 | 0.39 | 0.09 |
| | 2 | 3 | 0.65 | 0.06 |
| $H_2$ | 1 | 1.9 | 0.37 | 0.10 |
| | 2 | 3.3 | 0.61 | 0.05 |

[a] Number of phosphorus atoms. [b] Distance between Ni(I) and phosphorus; estimated uncertainty is ±0.01 nm. [c] Isotropic hyperfine coupling constant; estimated uncertainty is ±10%.

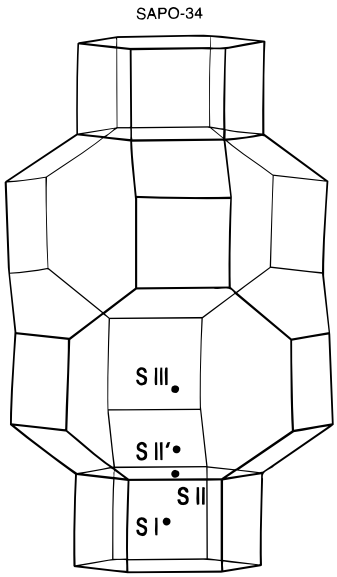


**Figure 9.** Structural model of SAPO-34 with possible cation positions shown. See text for description of the cation positions.

cation sites in SAPO-34 are shown in Figure 9 and can be described as follows. Site I is at the center of a hexagonal prism, site II is the center of a six-ring window, site II′ is displaced from a six-ring into the cavity, and site III is near the center of an eight-ring window. In zeolite chabazite, additional sites with low cation occupancy have also been reported.

The observance of $^{27}$Al modulation in hydrogen-reduced NiH−SAPO-34 indicates that the Ni ion is situated within 5 Å of framework aluminum.[26] Moreover, the fact that this modulation is quite shallow and extends to long values of $T$ implies that the magnetic nucleus is not in close proximity to the paramagnetic species.[27] This strengthens our assumption that in ion-exchanged samples Ni occupies extraframework sites. $^{31}$P modulation of NiH−SAPO-34 after dehydration at 773 K and after hydrogen reduction did not show noticeable differences, suggesting that species A formed by both reduction procedures is located in the same site in SAPO-34. Furthermore, simulation of these spectra shows two nearest-neighbor phosphorus atoms at 3.8 Å and three next-nearest-neighbor phosphorus atoms at about 6.0 Å. From the framework chemical composition of SAPO-34, there are 2−3 P nuclei, 3 Al nuclei, and 0−1 Si nuclei in a six-ring window of the framework. A six-ring window consisting of three phosphorus and three aluminums has no net framework charge. Therefore, it is likely that the positively charged nickel ion will locate near a negatively charged six-ring window with at least one silicon substituted for phosphorus. This site can be identified as site II′ in the chabazite cage near a six-ring window (Figure 9). Similar behavior has been reported in NiH−SAPO-41.[19] However, migration of metal ions from supercages and larger channels to smaller ones during dehydration is a common phenemenon in zeolites and other molecular sieves.[28] In low and intermediate silica zeolites, the high negative charge density in the small cavities and channels provides the main driving force for the migration of multivalent transition-metal ions from larger channels or supercages to smaller ones. In zeolite X and Y, metal ions initially located within the large supercage migrate to a smaller sodalite cage during dehydration. Similarly in SAPO-5 and SAPO-11, metal ions initially located in the large 12-ring or 10-ring channels migrate to smaller 6-ring channels during dehydration.[29] Since site II′ is a much more accessible site than is site I, this means that nickel-exchanged SAPO-34 should be a good catalyst candidate.

After reduction by $H_2$, Ni(I) ions are in site II′. Water adsorption produces a single Ni(I)−$(O_2)_n$ species. However, methanol adsorption gives rise to two Ni(I)−$(CD_3OH)_n$ complexes. It is likely that while some of the Ni(I) ions remain in site II′ to interact with the adsorbate, a fraction of Ni(I) ions migrate to another site where it forms another complex with methanol. The site to which these Ni(I) ions move is most likely site III, which is the center of an eight-ring window.

The equivalent interaction of three molecules of CO with 90% $^{13}$CO with Ni(I) in SAPO-34 generates the following relative hyperfine intensity distributions:

4.5:1:4.5 for a Ni(I)−$(CO)_3$ complex with one $^{13}$CO

2:1:4:1:2 for a Ni(I)−$(CO)_3$ complex with two $^{13}$CO

1.5:1:5:2:5:1:1.5 for a Ni(I)−$(CO)_3$ complex with three $^{13}$CO

The above figures take into account the isotopic distributions of the various species including $(^{13}CO)_0$−Ni(I)−$(^{12}CO)_3$, $(^{13}CO)_1$−Ni(I)−$(^{12}CO)_2$, $(^{13}CO)_2$−Ni(I)−$(^{12}CO)_1$, and $(^{13}CO)_3$−Ni(I)−$(^{12}CO)_0$.

The observed relative intensity distribution does not completely fit the theoretical one which does not take into account the line broadening with $M_I$, i.e., the line due to $^{12}$C ($I = 0$) labeled carbonyl species is not broadened in contrast to the other hyperfine lines. Previous results have shown that, for adsorption of CO on NiCa−X, Ni(I) ions migrate from inaccessible sodalite cages to accessible supercages where they coordinate to three framework oxygens.[10] In the supercages Ni(I) can reversibly coordinate with one to three CO molecules to form Ni(I)−(CO),

$Ni(I)-(CO)_2$, and $Ni(I)-(CO)_3$ complexes. Studies of CO adsorption on PdH−SAPO-34 indicate formation of a Pd(I) complex with three molecules of CO based on resolved $^{13}C$ superhyperfine splittings.[33]

Cupric ion studies in SAPO-17 showed that ethylene only coordinates to relatively exposed Cu(II) ions.[30] The kinetic diameter of ethylene (∼4 Å) is too large for it to enter the cancrinite cage for which the largest window is a six-ring with an effective diameter of ∼2.5 Å. So, ethylene cannot coordinate with Cu(II) ions which migrate to the cancrinite cage during dehydration.

Ethylene dimerization activity and selectivity have been reported on Ni(I) in ion-exchanged SAPO-5 and SAPO-11.[31] ESEM data indicated the coordination of one ethylene molecule and the formation of a $\pi$-bond between Ni(I) and $C_2D_4$ in NiH−SAPO-5 and NiH−SAPO-11. The same work pointed out that paramagnetic Ni(I) species are rather unstable toward traces of water and oxygen. Also, it was observed that Ni(I) can be reduced by ethylene or butenes to metallic nickel clusters,[32] implying that the active nickel cations are unstable under the reaction conditions and are likely converted to atomic Ni which is catalytically inactive for ethylene dimerization. It can also be expected that Ni(I) in an ion-exchanged site is even less stable toward reduction to Ni(0) than would be Ni(I) in a framework site because it is more accessible to reducing agents. All these observations are equally relevant in NiH−SAPO-34. However, in materials such as NiH−SAPO-5 and NiH−SAPO-11 where Ni migrates from the main channel to the center of a hexagonal prism after reduction, Ni(I) is less reactive toward ethylene than toward methanol. This can be explained by two facts. First, as has already been mentioned, ethylene and methanol are both too big to enter the hexagonal prism. Second, the lesser polarity of $C_2D_4$ compared to $CD_3OH$ makes it unable to pull Ni(I) out of a hexagonal prism.

In the present work, we suggest that the structure of small pore SAPO-34 gives rise to a different behavior from SAPO-5 and SAPO-11. Here, polarity considerations do not apply since Ni(I) is still located in the main cage after reduction. Therefore, it is understandable that no Ni(I) remains after ethylene adsorption onto reduced NiH−SAPO-34. SAPO-5 and SAPO-11 molecular sieves are structurally similar, both being channel-type structures which consist of 12-ring and 10-ring main channels, respectively, connected with four-ring and six-ring windows. SAPO-41 is also a medium-pore molecular sieve with adjacent 10-ring channels. However, SAPO-34, as already mentioned, has a cage-type structure with a large cavity inside the framework bordered by four-ring, six-ring, and eight-ring windows, which is quite different from the other SAPO materials previously investigated. This partly explains why Ni(I) in SAPO-34 behaves uniquely.

## Conclusions

Thermal, hydrogen, and $\gamma$-irradiation reduction procedures are effective to reduce Ni(II) to Ni(I) in NiH−SAPO-34. While thermal reduction and $\gamma$-irradiation produce a single Ni(I) species, two Ni(I) species are observed after hydrogen reduction. $Ni(I)-(O_2)_n$ is observed after adsorption of water, indicating decomposition of water. Adsorption of methanol produces two $Ni(I)-(CD_3OH)_n$ complexes, suggesting that Ni(I) coordinates to methanol from two different sites. Ni(I) interacts with ethylene to form two $Ni(I)-(C_2D_4)_n$ complexes. Carbon monoxide adsorption generates $Ni(I)-(CO)_3$ as observed in NiCa−X; such an interaction between Ni(I) and CO has not been reported before in SAPO materials. ESEM studies reveal that Ni(I) ions are primarily at site II′ near a six-ring window after reduction. The Ni(I) site in NiH−SAPO-34 after reduction is different from the site in NiH−SAPO-5 and NiH−SAPO-11 but is similar to the site observed in SAPO-41.

It is clear that several factors including the structure types and the pretreatment conditions determine the location of Ni(I) ions and the way they interact with adsorbates in molecular sieves. Thus, the behavior of a transition-metal ion exchanged into a particular molecular sieve is somewhat specific to that material justifying the study of a wide range of molecular sieve materials.

**Acknowledgment.** This research was supported by the National Science Foundation and the Robert A. Welch Foundation.

## References and Notes

(1) Wilson, S. T.; Lok, B. M.; Flanigen, E. M. U.S. Patent 4 310 440, 1982.
(2) Ishihara, T.; Kagawa, M.; Hadama, F.; Takita, Y. In *Zeolites and Related Micropororous Materials: State of the Art 1994*; Weitkamp, J.; Karge, H. G.; Pfeifer, H.; Holderich, W.; Eds.; Studies in Surface Science and Catalysis, Vol. 84; Elsevier: Amsterdam, 1994; pp 1493−1500.
(3) Inui, T.; Phatanasri, S.; Mutsuda, H. *J. Chem. Soc., Chem. Commun.* **1990**, 205.
(4) Lok, B. M.; Messina, C. A.; Patton, R. L.; Gajek, R. T.; Cannan, T. R.; Flanigen, E. M. *J. Am. Chem. Soc.* **1984**, *106*, 6092.
(5) Messina, C. A.; Lok, B. M.; Flanigen, E. M. U.S. Patent 4 544 143, 1985.
(6) Meier, W. M.; Olson, D. H.; Baerlocher, Ch. *Atlas of Zeolite Structure Types*, 4th ed.; Elsevier: London, 1996; pp 76−77.
(7) Xu, Y.; Grey, C. P.; Thomas, J. M.; Cheetham, A. K. *Catal. Lett.* **1990**, *4*, 251.
(8) Kazansky, V. B.; Elev, I. V.; Shelimov, B. N. *J. Mol. Catal.* **1883**, *21*, 265.
(9) Ghosh, A. K.; Kevan, L. *J. Phys. Chem.* **1990**, *94*, 3117.
(10) Kermarec, M.; Olivier, D.; Richard, M.; Chen, M. *J. Phys. Chem.* **1982**, *86*, 2818.
(11) Abou-Kais, A.; Vedrine, J. C.; Massardier, J.; Dalmai-Imelik, G. *J. Chem. Soc., Faraday Trans.* **1974**, *70*, 1039.
(12) Hartmann, M.; Azuma, N.; Kevan, L. *J. Phys. Chem.* **1995**, *99*, 10988.
(13) Azuma, N.; Lee, C. W.; Kevan, L. *J. Phys. Chem.* **1994**, *98*, 1217.
(14) Prakash, A. M.; Hartmann, M.; Kevan, L. *J. Chem. Soc., Faraday Trans.* **1997**, *93*, 1233.
(15) Prakash, A. M.; Unnikrishnan, S. *J. Chem. Soc., Faraday Trans*. **1994**, *90*, 2291.
(16) Lok, B. M.; Messina, C. A.; Patton, R. L.; Gajek, R. T.; Cannon, T. R.; Flanigen, E. M. U.S. Patent 4 440 871, 1984.
(17) Azuma, N.; Kevan, L. *J. Phys. Chem.* **1995**, *99*, 5083.
(18) Azuma, N.; Hartmann, M.; Kevan, L. *J. Phys. Chem.* **1995**, *99*, 6670.
(19) Prakash, A. M.; Wasowicz, T.; Kevan, L. *J. Phys. Chem.* **1996**, *100*, 15947.
(20) Suk, B. H.; Sun, J. K.; Uh, Y. S. *J. Phys. Chem.* **1996**, *100*, 15923.
(21) Garbowski, E. D.; Mathieu, M. V.; Primet, M. *Chem. Phys. Lett.* **1977**, *49*, 247.
(22) Michalik, J.; Narayama, M.; Kevan, L. *J. Phys. Chem.* **1984**, *88*, 5236.
(23) Schoonheydt, R. A.; Vaesen, I.; Leeman, H. *J. Phys. Chem.* **1989**, *93*, 1515.
(24) Olivier, D.; Richard, M.; Che, M. *Chem. Phys. Lett.* **1978**, *60*, 77.
(25) Mortier, W. J. *Compilation of Extraframework Sites in Zeolites*; Structure Commission of the International Zeolite Association; Butterworth: Surrey, 1982; pp 11−12.
(26) Sass, C. E.; Kevan, L. *J. Phys. Chem.* **1988**, *92*, 14.
(27) Sass, C. E.; Kevan, L. *J. Phys. Chem.* **1989**, *93*, 7856.
(28) Sachtler, W. M. H.; Zhang, Z. *Adv. Catal.* **1993**, *39*, 129.
(29) Lee, C. W.; Chen, X.; Kevan, L. *Catal. Lett.* **1992**, *15*, 75.
(30) Prakash, A. M.; Kevan, L. *Langmuir* **1997**, *13*, 5341.
(31) Hartmann, M.; Kevan, L. *J. Chem. Soc., Faraday Trans.* **1996**, *92*, 1429.
(32) Coughlan, B.; Keane, M. A. *J. Catal.* **1990**, *123*, 264.
(33) Back, G. H.; Yu, J. S.; Kurshev, V.; Kevan, L. *J. Chem. Soc., Faraday Trans.* **1994**, *90*, 2283.